



**HAL**  
open science

# Temporal upscaling of instantaneous evapotranspiration on clear-sky days using the constant reference evaporative fraction method with fixed or variable surface resistances at two cropland sites

Ronglin Tang, Zhao-Liang Li, Xiaomin Sun, Yuyun Bi

## ► To cite this version:

Ronglin Tang, Zhao-Liang Li, Xiaomin Sun, Yuyun Bi. Temporal upscaling of instantaneous evapotranspiration on clear-sky days using the constant reference evaporative fraction method with fixed or variable surface resistances at two cropland sites. *Journal of Geophysical Research: Atmospheres*, 2017, 122 (2), pp.784-801. <10.1002/2016JD025975>. <hal-03527247>

**HAL Id: hal-03527247**

**<https://hal.science/hal-03527247v1>**

Submitted on 15 Jan 2022

HAL is a multi-disciplinary open access archive for the deposit and dissemination of scientific research documents, whether they are published or not. The documents may come from teaching and research institutions in France or abroad, or from public or private research centers.

L'archive ouverte pluridisciplinaire HAL, est destinée au dépôt et à la diffusion de documents scientifiques de niveau recherche, publiés ou non, émanant des établissements d'enseignement et de recherche français ou étrangers, des laboratoires publics ou privés.



HAL Authorization

1 **Temporal upscaling of instantaneous evapotranspiration on clear-sky days using the**  
2 **constant reference evaporative fraction method with fixed or variable surface**  
3 **resistances at two cropland sites**

4 **Ronglin Tang<sup>1</sup>, Zhao-Liang Li<sup>2,3,\*</sup>, Xiaomin Sun<sup>4</sup> and Yuyun Bi<sup>2</sup>**

5 <sup>1</sup>State Key Laboratory of Resources and Environment Information System, Institute of  
6 Geographic Sciences and Natural Resources Research, Beijing 100101, China.

7 <sup>2</sup>Key Laboratory of Agri-informatics, Ministry of Agriculture/Institute of Agricultural Resources  
8 and Regional Planning, Chinese Academy of Agricultural Sciences, Beijing 100081, China.

9 <sup>3</sup>ICube, UdS, CNRS; 300 Bld Sebastien Brant, CS10413, 67412 Illkirch, France.

10 <sup>4</sup>Key Laboratory of Ecosystem Network Observation and Modeling, Institute of Geographic  
11 Sciences and Natural Resources Research, Beijing 100101, China.

12 Corresponding author: Zhao-Liang Li ([lizhaoliang@caas.cn](mailto:lizhaoliang@caas.cn))

13 **Key Points:**

- 14 • The constant reference evaporative fraction upscaling method was tested.  
15 • Fixed and variable surface resistances were compared in the ET upscaling.  
16 • Analysis was made over different assumed satellite overpass times.  
17

## 18 Abstract

19 Surface evapotranspiration (ET) is an important component of water and energy in land and  
20 atmospheric systems. This paper investigated whether using variable surface resistances in the  
21 reference ET estimates from the full-form Penman-Monteith (PM) equation could improve the  
22 upscaled daily ET estimates in the constant reference evaporative fraction ( $EF_r$ , the ratio of  
23 actual to reference grass/alfalfa ET) method on clear-sky days using ground-based  
24 measurements. Half-hourly near-surface meteorological variables and eddy covariance (EC)  
25 system-measured latent heat flux data on clear-sky days were collected at two sites with different  
26 climatic conditions, namely, the sub-humid Yucheng station in northern China and the arid  
27 Yingke site in northwestern China and were used as the model input and ground-truth,  
28 respectively. The results showed that using the FAO-PM equation, the ASCE-PM equation, and  
29 the full-form PM equation to estimate the reference ET in the constant  $EF_r$  method produced  
30 progressively smaller upscaled daily ET at a given time from mid-morning to mid-afternoon.  
31 Using all three PM equations produced the best results at noon at both sites regardless of whether  
32 the energy imbalance of the EC measurements was closed. When the EC measurements were not  
33 corrected for energy imbalance, using variable surface resistance in the full-form PM equation  
34 could improve the ET upscaling in the mid-afternoon, but worse results may occur in the mid-  
35 morning to noon. Site-to-site and time-to-time variations were found in the performances of a  
36 given PM equation (with fixed or variable surface resistances) before and after the energy  
37 imbalance was closed.

38 **Key words:** evapotranspiration; reference evaporative fraction method; temporal upscaling;  
39 fixed or variable resistance

## 40 1 Introduction

41 Land surface evapotranspiration (ET, water in mm equivalent to latent heat flux) is one of  
42 the most significant components of the global hydrological cycle, and its estimation plays a  
43 significant role in numerical weather forecasting, global climate change modeling, and irrigation  
44 water allocation. Although many eddy covariance sites have been established worldwide in the  
45 past several decades to measure the long-term transfer of surface water, heat, and momentum  
46 across different ecosystems [Baldocchi *et al.*, 2001], these measurements are spatially discrete  
47 and of limited spatial representativeness. Remote sensing technology provides the ability to map  
48 surface ET over large heterogeneous areas and complements conventional ground-based ET  
49 measurements at the tower scale. Because remote sensing models of ET estimation can generally  
50 only provide instantaneous values at the clear-sky satellite overpass time [Kalma *et al.*, 2008; Li  
51 *et al.*, 2009; Tang *et al.*, 2010, 2012], several upscaling methods have been developed to convert  
52 instantaneous ET data to a daily value so that water consumption by crops can be monitored  
53 [Shuttleworth *et al.*, 1989; Trezza, 2002; Jackson *et al.*, 1983; Brutsaert and Sugita, 1992; Ryu *et al.*  
54 *et al.*, 2012; Van Niel *et al.*, 2012; Delogu *et al.*, 2012].

55 The constant reference evaporative fraction [ $EF_r$ , the ratio of actual to reference grass  
56 (alfalfa) ET] method, which was proposed by Trezza [2002] to use a fixed surface resistance of  
57 50 (30) s/m during the daytime and 200 s/m during the nighttime for reference grass (alfalfa) ET  
58 estimates and assumes that  $EF_r$  is relatively constant during the day, is one of the most widely  
59 applied schemes for upscaling instantaneous remote sensing estimates of ET. The effectiveness  
60 of the constant  $EF_r$  method in upscaling instantaneous ET data has been investigated and  
61 demonstrated by numerous studies that used primarily local (in-situ) metrological observations

62 [Colaizzi *et al.*, 2006; Chávez *et al.*, 2008; Allen *et al.*, 2007; Liu *et al.*, 2012; Tang *et al.*, 2013a].  
63 Biases may be found when this method is tested using only remote sensing data [Cammalleri *et al.*, 2014].  
64

65 The key to using the constant  $EF_r$  method is to accurately estimate the instantaneous (or  
66 half-hourly/hourly) and daily ET values for a reference crop using the Penman-Monteith (PM)  
67 equation. A fixed surface resistance of 70 s/m was adopted by FAO56 for the reference grass ET  
68 estimate from the PM (hereafter referred to as FAO-PM) equation for hourly and daily time steps  
69 [Allen *et al.*, 1998]. By comparing the major reference ET equations using weather data from  
70 diverse climates across the United States, the Environmental and Water Resources Institute of  
71 the American Society of Civil Engineers [ASCE-EWRI, 2005] recommended using a fixed  
72 surface resistance of 50 s/m during the daytime and 200 s/m during the nighttime for shorter  
73 reference grass ET estimates from the PM (hereafter referred to as ASCE-PM) equation at hourly  
74 or shorter computation steps.

75 Surface resistance not only is a physiological parameter but also has an aerodynamic  
76 component. The surface resistance over the course of a day is essentially time-dependent and can  
77 be influenced by variations in solar radiation, vapor pressure deficit, and wind speed even for the  
78 water-unstressed reference grass/alfalfa surface. Katerji and Perrier [1983] related the surface  
79 resistance to aerodynamic resistance and climatological variables through a linear model.  
80 However, the coefficients in their model must be experimentally calibrated before they can be  
81 applied to grass and alfalfa. Alves and Pereira [2000] reported that the model can be applied  
82 only under a limited range of Bowen ratio conditions. Todorovic [1999] also modeled the surface  
83 resistance as a function of aerodynamic resistance and climatic variables, but his model does not  
84 require a priori calibration and can be applied without additional constraints. Both surface  
85 resistance models have been widely used in the application of the PM equation, and several  
86 authors have recommended them for practical use because they provide better estimates of the  
87 reference ET than using a fixed value of 70 s/m [Pereira *et al.*, 1999; Rana and Kaerji, 2000;  
88 Lecina *et al.*, 2003; Perez *et al.*, 2006; Liu *et al.*, 2012].

89 To the best of our knowledge, almost all recent investigations of the constant  $EF_r$  upscaling  
90 method have used a fixed surface resistance of 50 s/m during the daytime periods to estimate the  
91 reference short grass (or 30 s/m for the reference tall alfalfa) ET as recommended by the ASCE-  
92 EWRI [Colaizzi *et al.*, 2006; Allen *et al.*, 2007; Chávez *et al.*, 2008; Tang *et al.*, 2013a]. No  
93 studies have ever attempted to incorporate a variable daytime surface resistance in the upscaling  
94 of instantaneous ET data using the constant  $EF_r$  method. Similar upscaled daily ET results can be  
95 expected to be obtained when the daytime variable surface resistance is close to the fixed values  
96 of 70 s/m in the FAO-PM equation or 50 s/m in the ASCE-PM equation. Additional studies are  
97 necessary to assess the performance of the constant  $EF_r$  upscaling method under extreme climatic  
98 conditions, when the variable surface resistance significantly deviates from the commonly used  
99 fixed value.

100 The objective of this study is to use ground-based measurements to investigate whether  
101 using a variable surface resistance in the reference ET estimate from the PM equation can  
102 improve the daily (24-h) upscaled ET result of the constant  $EF_r$  method. Section 2 describes the  
103 derivation of the variable surface resistance, the formulations of the three reference ET  
104 estimation methods, and the ET-upscaling theory. Section 3 presents the validation sites, the  
105 procedures for selecting clear days during each of the three daytime periods, and the method of  
106 correcting the energy imbalance in the EC-measured fluxes. In section 4, the daily ETs that are

107 upscaled using the three reference ET estimation methods are compared and validated. A  
 108 summary and conclusions are provided in Section 5.

## 109 2 Methodology

### 110 2.1 Derivation of variable surface resistance

111 Based on the principle of surface energy balance, the difference between the potential ET  
 112 and actual ET (reference ET in this paper) can be assumed to be caused by an additional sensible  
 113 heat flux imposed to heat the vegetation surface to provide the extra energy to move saturated air  
 114 out of vegetation elements. *Todorovic* [1999] predicted this additional sensible heat flux as a  
 115 function of a “pseudo” resistance to the additional sensible heat transfer and the difference  
 116 between the temperature on the potential ET surface and that on the actual ET surface. With the  
 117 assumption that the “pseudo” resistance equals the surface resistance and the temperature  
 118 difference is approximated as a function of the vapor pressure deficit and air temperature, the  
 119 surface resistance can be estimated by combining the ET estimated from the PM equation and  
 120 the additional sensible heat into the surface energy balance equation. A detailed description of  
 121 the theory and development of the model can be found in *Todorovic* [1999]. Here, we focus on  
 122 the formulations that are used to obtain the surface resistance. In *Todorovic*’s method, the  
 123 variable surface resistance during the daytime can be solved through the following quadratic  
 124 equation:

$$125 \quad a\left(\frac{r_s}{r_c}\right)^2 + b\frac{r_s}{r_c} + c = 0 \quad (1)$$

126 where  $r_s$  is the surface resistance, s/m; and  $r_c$  is the climatological resistance, s/m. The  
 127 coefficients  $a$ ,  $b$ , and  $c$  and the climatological resistance can be derived as follows:

$$r_c = \rho c_p \frac{e_s - e_a}{\gamma \times E} \quad (2)$$

$$a = \frac{\Delta + \gamma(r_c / r_a)}{\Delta + \gamma} (r_c / r_a)(e_s - e_a) \quad (3)$$

$$b = -\gamma \frac{e_s - e_a}{\Delta + \gamma} \frac{r_c}{r_a} \frac{\gamma}{\Delta} \quad (4)$$

$$c = -(\Delta + \gamma) \frac{e_s - e_a}{\Delta + \gamma} \frac{\gamma}{\Delta}, \quad (5)$$

128 where  $\Delta$  is the slope of the saturated vapor pressure versus the air temperature curve, kPa/°C;  $\rho$  is  
 129 the air density, kg/m<sup>3</sup>;  $c_p$  is the specific heat of the air, J/(kg·°C);  $e_s - e_a$  is the vapor pressure  
 130 deficit of the air, kPa;  $\gamma$  is the psychrometric constant, kPa/°C;  $E$  is the surface available energy  
 131 and equals surface net radiation minus soil heat flux, W/m<sup>2</sup>; and  $r_a$  is the aerodynamic resistance,  
 132 s/m. Eq. (1) has only one positive surface resistance solution.

## 133 2.2 Estimation of Reference ET

### 134 2.2.1 Full-form PM equation

135 Using the solved variable surface resistance from Eq. (1) at the hourly (or half-hourly) time  
136 scale, the reference ET during the daytime can be derived from the “full-form” PM combination  
137 equation:

$$138 \quad ET_{TOD-PM} = \frac{\Delta(R_n - G) + \rho c_p (e_s - e_a) / r_a}{\Delta + \gamma(1 + r_s / r_a)} \quad (6)$$

139 where  $R_n$  is the surface net radiation;  $G$  is the soil heat flux;  $ET_{TOD-PM}$  is the reference ET  
140 estimated using the variable surface resistance that is derived from Todorovic’s method.

141 A short reference crop and a tall reference crop, as proposed by *ASCE-EWRI* [2005], are  
142 adopted to estimate the reference ET for wheat and corn, respectively. When the full-form PM  
143 equation is applied to the reference short/tall crop, this equation can be reduced to a simplified  
144 form given that  $r_a$  can be estimated with the procedure presented by *Allen et al.* [1998]. The  
145 simplified PM equation can be expressed as

$$ET_{TOD-PM} = \frac{0.408\Delta(R_n - G) + \gamma \frac{C_n}{T_a + 273} u_2 (e_s - e_a)}{\Delta + \gamma(1 + C_d u_2)}, \quad (7)$$

$$C_d u_2 = r_s / r_a = \begin{cases} \frac{u_2}{208} r_s & \text{short grass} \\ \frac{u_2}{118} r_s & \text{tall alfalfa} \end{cases}, \quad (8)$$

146 where  $R_n$  and  $G$  are expressed in units of MJ/(m<sup>2</sup>·d);  $u_2$  is the wind speed measured at 2 m  
147 height, m/s;  $T_a$  is the air temperature, °C; and  $C_n$  and  $C_d$  are the coefficients that change with  
148 surface resistance. For the reference short grass,  $C_n$  equals 900 at the daily scale and 37 at the  
149 hourly scale. For the reference tall alfalfa,  $C_n$  equals 1600 at the daily scale and 66 at the hourly  
150 scale. From Eq. (8),  $r_a$  equals 208/ $u_2$  for short grass and 118/ $u_2$  for tall alfalfa. During the  
151 nighttime period, the surface resistance is fixed at 200 s/m for both reference surfaces, as is done  
152 in the ASCE-PM equation (see Section 2.2.3). With the exception of the surface resistance, the  
153 calculation of each of the variables in Eq. (7) closely follows the procedures specified by *ASCE-*  
154 *EWRI* [2005].

### 155 2.2.2 FAO-PM equation

156 In the standard FAO-PM equation [*Allen et al.*, 1998], the reference ET is estimated with  
157 the simplified PM equation for a hypothetical grass (or alfalfa) with an assumed height of 0.12 m  
158 (or 0.5 m), a fixed surface resistance of 70 (or 45) s/m, and an albedo of 0.23 for both the daily  
159 and hourly time steps. The FAO-PM equation has the same formulation as Eq. (7). The only  
160 difference is that the coefficient  $C_d$  equals 0.34 for the reference short grass and 0.38 for the  
161 reference tall alfalfa for a daily cycle in the FAO-PM equation.

### 162 2.2.3 ASCE-PM equation

163 In the standard ASCE-PM equation [ASCE-EWRI, 2005] for the reference short grass (tall  
164 alfalfa), the fixed resistance of 70 (45) s/m used in the FAO-PM equation is replaced by a lower  
165 value of 50 (30) s/m during the daytime and a higher value of 200 s/m during the nighttime. The  
166 ASCE-PM equation also has the same formulation as Eq. (7). The only difference is that the  
167 coefficient  $C_d$  equals 0.24 (0.25) during daytime and 0.96 (1.7) during nighttime for the reference  
168 short grass (tall alfalfa) in the ASCE-PM equation.

### 169 2.3. Upscaling of instantaneous ET

170 After the half-hourly or hourly reference ET value is estimated with the three PM equations,  
171 assuming that the ratio of the actual instantaneous ET to daily ET values equals the ratio of the  
172 corresponding reference instantaneous ET to daily ET values, the actual daily ET can be derived  
173 as follows:

$$ET_{a,d} = \frac{ET_{r,d}}{ET_{r,i}} ET_{a,i} \quad (9)$$

174 where  $ET_{r,i}$  and  $ET_{a,i}$  are the reference ET value and the actual ET value at the instantaneous time  
175 scale, respectively;  $ET_{r,d}$  and  $ET_{a,d}$  are the reference ET value and the actual ET value at the daily  
176 (24-h) time scale, respectively. The  $ET_{r,i}$  can be estimated from the full-form PM equation, the  
177 FAO-PM equation, or the ASCE-PM equation; the  $ET_{r,d}$  is estimated by summing the half-hourly  
178  $ET_{r,i}$  values over a diurnal cycle. The  $ET_{a,i}$  comes from the half-hourly ground-based eddy  
179 covariance measurements that are uncorrected for energy imbalance or corrected by the Bowen  
180 ratio and the residual energy methods (see Section 3.3).

## 181 3 Test site and data

### 182 3.1 Test site

183 Data were collected at two sites (Yucheng and Yingke; see Table 1), which are  
184 characterized by contrasting climatic conditions in China, to investigate the use of the constant  
185  $EF_r$  method to upscale instantaneous ET data. The Yucheng site is located in the North China  
186 Plain and has a sub-humid monsoon climate and a sandy loam soil texture. Winter wheat  
187 (October to June) and summer corn (June to October) are rotated each year. Approximately 60-  
188 70% of the annual rainfall occurs during the summer corn growing season, and the remaining 30-  
189 40% falls during the winter wheat growing season. The Yingke site is located in an irrigated field  
190 in the middle reaches of the Heihe River Basin in northwestern China and is characterized by an  
191 arid climate and a silt loam soil texture. Corn is interplanted with spring wheat from May to July  
192 and the site is covered by corn only from August to September.

193 Both sites are equipped with standard sensors (Table 2) that measure meteorological  
194 variables (e.g., air temperature, air pressure, actual vapor pressure, and wind speed/direction) and  
195 the soil water and temperature profiles at 30-min intervals. Downward and upward shortwave  
196 and longwave radiation are measured with a CNR-1 device at both sites, and the soil heat flux  
197 ( $G$ ) is measured with an HFP-01 soil heat flux plate at a depth of 2 cm at the Yucheng site and 5  
198 cm at the Yingke site. Heat storage above the plate is not accounted for because no more  
199 information is available at hand for its correction. Over the entire study period, the multi-day  
200 mean surface available energy ( $R_n - G$ ) at the Yingke site is much larger than that at the Yucheng

201 site; the difference can be as much as  $\sim 100 \text{ W/m}^2$  at noon (see Figure 1a). In contrast, the multi-  
 202 day mean wind speed ( $u$ ) at the Yingke site is  $\sim 1.3 \text{ m/s}$  lower than that at the Yucheng site  
 203 (Figure 1b). Moreover, the maximum wind speed at the Yucheng site generally occurs at noon,  
 204 whereas the maximum wind at the Yingke site occurs in the mid-afternoon. The daytime wind  
 205 speed at the Yingke site is more asymmetric than that at the Yucheng site. The multi-day mean  
 206 vapor pressure deficit ( $VPD$ ) at the Yingke site is slightly higher than that at the Yucheng site  
 207 and has a maximum value of  $\sim 1.5 \text{ kPa}$ . Over the involved clear-sky days (see Section 3.2 for the  
 208 selection rules) that are selected for the model assessment, the multi-day mean surface available  
 209 energy is slightly and moderately (difference  $< 70 \text{ W/m}^2$ ) larger at the Yingke site and Yucheng  
 210 site, respectively, than that over the entire study period from mid-morning to mid-afternoon. The  
 211 multi-day mean surface available energy at the Yingke site is still larger than that at the Yucheng  
 212 site, but their difference ( $< 50 \text{ W/m}^2$ ) becomes smaller than that over the entire study period. The  
 213 multi-day mean wind speed at the Yucheng and Yingke sites over the selected clear-sky days is  
 214 moderately higher than (difference  $< 0.6 \text{ m/s}$ ) and has a similar magnitude to that over the entire  
 215 study period, respectively, which causes a much larger difference (as high as  $1.8 \text{ m/s}$ ) in wind  
 216 speed between the Yucheng site and the Yingke site over the selected clear-sky days. Both the  
 217 Yucheng and the Yingke sites have slightly larger multi-day mean  $VPD$  over the selected clear-  
 218 sky days than over the entire study period from the mid-morning to mid-afternoon. A negligible  
 219 difference is observed in the multi-day mean  $VPD$  between the Yucheng and the Yingke sites  
 220 over the selected clear-sky days.  
 221

222 **Table 1.** Attributes of the two sites in China used for the evaluation of the constant reference  
 223 evaporative fraction upscaling method (AP: Annual mean precipitation, mm; AT: Annual  
 224 mean temperature,  $^{\circ}\text{C}$ )

Site	Longitude (E)	Latitude (N)	Land cover	Elevation(m)	AP	AT	Data period
Yucheng	116.5703	36.8291	Crop	28	582	13.1	04/2009-06/2012
Yingke	100.4103	38.8571	Crop	1519	127	7.2	01/2008-11/2009

225  
 226  
 227

228 **Table 2.** Description of the model, manufacturer, and location for the instruments/sensors at the Yucheng [Yu et al., 2007; Sun et  
 229 al., 2009] and the Yingke [Liu et al., 2011] sites involved in this study.  $T_a$  and  $e_a$ : air temperature and actual vapor pressure;  $u$ :  
 230 wind speed;  $WD$ : wind direction;  $R_s$ : shortwave radiation;  $R_l$ : longwave radiation;  $G$ : soil heat flux;  $Pa$ : atmospheric pressure;  $T_s$ :  
 231 soil temperature;  $SM$ : soil moisture; H and LE: sensible and latent heat fluxes.

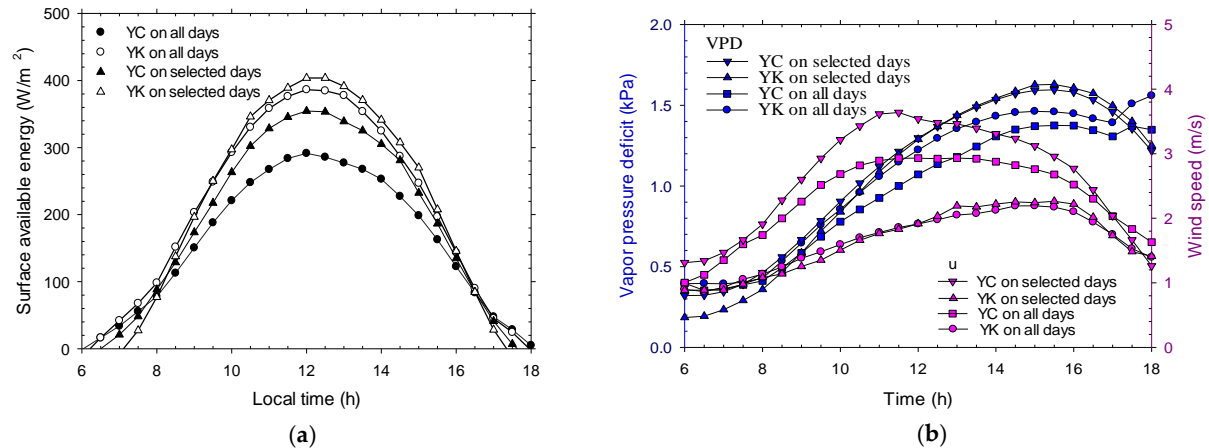
Site	$T_a$ and $e_a$	$u$	$WD$	$R_s$	$R_l$	$G$	$Pa$	$T_s$	$SM$	H and LE
Yucheng	HMP45C, Vaisala, Helsinki, Finland	A100R, Vector Instruments, Rhyl, UK	W200P, Vector Instruments, Rhyl, UK	CNR-1, Kipp & Zonen, Delft, Netherlands	CNR-1, Kipp & Zonen, Delft, Netherlands	HFP01, HUKSEFLUX, Delft, Netherlands	CS105, VAISALA, Helsinki, Finland	STP01, HUKSEFLUX, Delft, Netherlands	CS616, Campbell Scientific, Utah, USA	CSAT3/LI- 7500, Campbell Scientific /Li-Cor, Utah/ Nebraska, USA
		010C-1, Metone Instruments, Oregon, USA	020C-1, Metone Instruments, Oregon, USA	CM3, Kipp & Zonen, New York, USA	CG3, Kipp & Zonen, New York, USA	HFP01, Campbell Scientific, Utah, USA	CS100, Campbell Scientific, Utah, USA	109, Campbell Scientific, Utah, USA		

232

233

234 **Table 3.** Number of the clear-sky and partly cloudy days that had clear skies at three different daytime periods from April 2009 to  
 235 June 2012 at the Yucheng site and from January 2008 to November 2009 at the Yingke site.

Site	Time period		
	10:00-11:00	12:00-13:00	14:00-15:00
Yucheng	77	68	100
Yingke	76	73	80



236 **Figure 1.** Daytime variations of ground-based measurements of (a) surface available energy ( $R_n -$   
 237  $G$ ), (b) vapor pressure deficit ( $VPD$ ) and wind speed ( $u$ ), averaged from April 1, 2009 to June 30,  
 238 2012 or over the selected 125 clear-sky days at the Yucheng (YC) site and from January 1, 2008  
 239 to November 30, 2009 or over the selected 93 clear-sky days at the Yingke (YK) site.

240 The thirty-minute averaged sensible heat flux ( $H$ ) and latent heat flux ( $LE$ ) are regularly  
 241 measured by an eddy covariance ( $EC$ ) system that consists of an open-path  $CO_2/H_2O$  gas  
 242 analyzer (model LI-7500, Licor Inc., Lincoln, Nebraska) and a 3-D sonic  
 243 anemometer/thermometer (model CSAT3, Campbell Scientific Inc., Logan, Utah) at both sites.  
 244 The  $EC$  sensor is elevated to  $\sim 4.3$  m above surface level (ASL) in late July or early August and is  
 245 lowered to  $\sim 2.9$  m ASL in mid- to late-October every year at the Yucheng site but is fixed at  
 246  $\sim 2.8$  m ASL at the Yingke site. At the Yucheng and Yingke sites, the relative height of the  $EC$   
 247 sensor is  $\sim 2.1$  m and  $\sim 1.8$  m above maximum wheat height and  $\sim 1.7$  m and  $\sim 1.0$  m above the  
 248 maximum corn height, respectively. The main contributing area of the  $EC$  measurements is  
 249 within 180 m and 100 m around the sensor at the Yingke and Yucheng sites [Liu *et al.*, 2011;  
 250 Tang *et al.*, 2011a], respectively. To obtain reliable  $EC$ -measured  $H$  and  $LE$  data using the online  
 251 flux computation and post-field data programs [Yu *et al.*, 2006; Liu *et al.*, 2011], a series of  
 252 corrections are performed on the effect of the sonic virtual temperature, the time-lag, the  
 253 performance of the planar fit coordinate rotation, the density fluctuation, and the frequency  
 254 response following Webb *et al.* [1980] and Burba and Anderson [2010].

255 Half-hourly averaged atmospheric variables (global solar radiation, air temperature, wind  
 256 speed, relative humidity, and atmospheric pressure) were collected from April 2009 to June 2012  
 257 at the Yucheng site and from January 2008 to November 2009 at the Yingke site. The data were  
 258 used to drive the reference  $ET$  model and the daily (24-h) averaged latent heat flux measured by  
 259 the  $EC$  with and without an energy imbalance correction to validate the upscaled value from the  
 260 constant  $EF_r$  method. These data were carefully checked to ensure the quality and completeness  
 261 of the daily cycle in two steps. First, data spikes and abnormalities in the measured  $H$  and  $LE$   
 262 (less than  $-100$   $W/m^2$  or greater than  $700$   $W/m^2$  [Tang *et al.*, 2013; Liu *et al.*, 2011], which  
 263 approximate the lower and upper limits of surface net radiation) were removed, and then days  
 264 with data gaps caused by rainfall events, instrument malfunctions or maintenance, and data  
 265 spikes and abnormalities in the 30-min averaged atmospheric variables or  $EC$ -measured  $H$  and  
 266  $LE$  were excluded. After these data quality and completeness checks, 485 days from April 2009  
 267 to June 2012 at the Yucheng site and 272 days from January 2008 to November 2009 at the  
 268 Yingke site were available for further analysis. The daily measured surface fluxes (surface net

269 radiation, soil heat flux, sensible heat flux, and latent heat flux) can be obtained by averaging the  
270 48 half-hourly measurements of each diurnal cycle.

### 271 3.2 Selection of days with a clear sky at the assumed “satellite overpass” time

272 To recognize the possible time dependencies of the uncertainties and errors, the  
273 instantaneous ET values from three daytime periods (10:00-11:00, 12:00-13:00, and 14:00-15:00  
274 local time) between mid-morning and mid-afternoon, which correspond to the overpass times of  
275 most of the polar-orbiting satellites, were upscaled. The upscaling of the instantaneous ET data is  
276 generally restricted to clear-sky satellite overpass times in practical applications [Li *et al.*, 2013a,  
277 2013b]. The evaluation at both sites therefore focuses on days that have clear skies at the  
278 assumed satellite overpass times. Because the climatological resistance in the denominator on the  
279 left-hand side of Eq. (1) cannot equal zero, the relative humidity of the atmosphere during the  
280 daytime period for a given selected clear or partly cloudy day should be less than 100%, as seen  
281 in Eq. (2), which leads to a reduction in the available days to 355 days at the Yucheng site and  
282 208 days at the Yingke site. Though some authors have suggested estimating potential surface  
283 solar radiation as a factor of extraterrestrial radiation [e.g., Allen *et al.* [1998] assigned this factor  
284 to be 0.75 at sea level and incorporated the elevation to this factor above this level], the ratio of  
285 the observed clear-sky solar radiation to extraterrestrial radiation in previous studies [Todorovic  
286 *et al.*, 1999] and at the two sites in this study is shown to vary diurnally and seasonally.  
287 Determining whether a day is clear by comparing the observed surface solar radiation to the  
288 potential surface solar radiation determined as a fixed factor of extraterrestrial radiation is likely  
289 to miss some days. Here, we briefly review the two-step procedure that was proposed by Tang *et al.*  
290 [2013a] to identify the days that have clear skies at the different time intervals.

291 First, days that are clear during the entire daytime period are selected by analyzing the  
292 observed half-hourly global solar radiation and the corresponding shortwave atmospheric  
293 transmissivity ( $\tau$ , the ratio of the observed global solar radiation to the extraterrestrial solar  
294 radiation). If both values on a given day increase monotonically from sunrise (global solar  
295 radiation  $> 5 \text{ W/m}^2$ ) to midday and then decrease monotonically from midday to sunset (global  
296 solar radiation  $> 5 \text{ W/m}^2$ ), then that day will be classified as a clear-sky day and will be used for  
297 further analysis. Moreover, a visual check is made of the selected clear-sky days to remove those  
298 that are covered by constant cloud cover during the daytime.

299 Next, days that are partly cloudy during the daytime but have clear skies at the assumed  
300 satellite overpass times are selected. Days that do not have clear skies or constant cloud cover  
301 over the entire daytime period are classified as partly cloudy days. For each of the three different  
302 daytime periods, if the vertical-path shortwave atmospheric transmissivity ( $\tau_0 = \tau^{\cos\theta}$ , where  $\tau$  is  
303 the slant-path transmissivity at the solar zenith angle  $\theta$ ) on a given partly cloudy day is greater  
304 than the minimum of the corresponding  $\tau_0$  from two adjacent clear days, then that partly cloudy  
305 day will be selected for further analysis.

306 With the constraints provided by these selection criteria, 77 (76) clear-sky and partly cloudy  
307 days had clear skies at 10:00-11:00, 68 (73) days were clear at 12:00-13:00, and 100 (80) days  
308 were clear at 14:00-15:00 at the Yucheng (Yingke) site (see Table 3). The half-hourly  
309 meteorological variables and turbulent heat fluxes on these days were used to evaluate and  
310 validate the constant  $EF_r$  method.

### 311 3.3 Correction of the energy imbalance in the EC measurements

312 The energy imbalance in surface EC measurements has been reported in numerous studies  
313 [Twine *et al.*, 2000; Wilson *et al.*, 2002; Foken, 2008; Tang *et al.*, 2011b, 2013b; Stoy *et al.*,  
314 2013]. In most cases, the sum of the measured H and LE is less than the measured surface  
315 available energy. Although no consensus has been reached on how to best reconcile this energy  
316 imbalance, the Bowen ratio (BR) correction method and the residual energy (RE) correction  
317 method, which were proposed by Twine *et al.* [2000] and have been widely applied in previous  
318 years, are adopted in this study to correct the daytime 30-min averaged EC measurements to  
319 evaluate the  $EF_r$  upscaling method under energy-closure conditions. In the BR correction  
320 method, the surface available energy is repartitioned into H and LE by conserving the original  
321 EC-measured Bowen ratio. In the RE correction method, all of the imbalanced energy goes into  
322 the measured LE. When the RE correction method is directly applied to each of the  
323 corresponding 30-min averaged LE measurements in a diurnal cycle, the daily LE after  
324 correction averaged over the clear-sky or partly cloudy days is shown to be less than that before  
325 correction due to the negative available energy during the nighttime, which seems unreliable and  
326 is primarily caused by the limitation of the correction method during the nighttime. Moreover,  
327 the BR correction method is found to be corrupted if the sum of the original H and LE is close to  
328 zero during the nighttime. Therefore, we assume that the ratio of the EC-measured daytime to  
329 daily LE before and after the correction is constant to derive the corrected daily LE measurement  
330 after applying the BR and RE correction methods to the daytime 30-min averaged EC  
331 measurements.

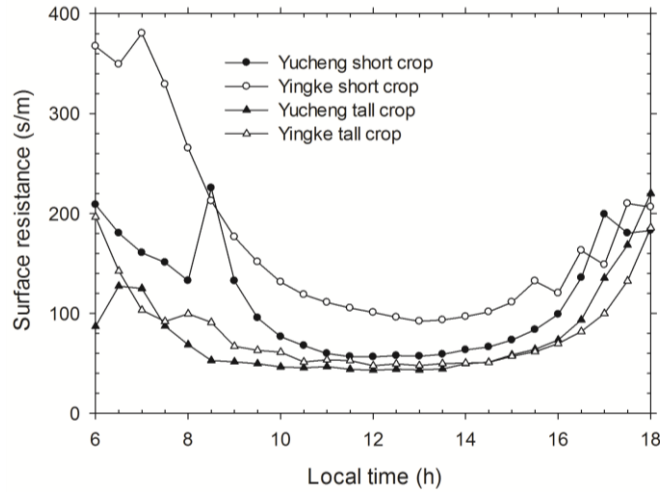
## 332 4 Results and discussion

### 333 4.1 Daytime variation in Todorovic's surface resistance and the noon-time evolution of the flux 334 ratio

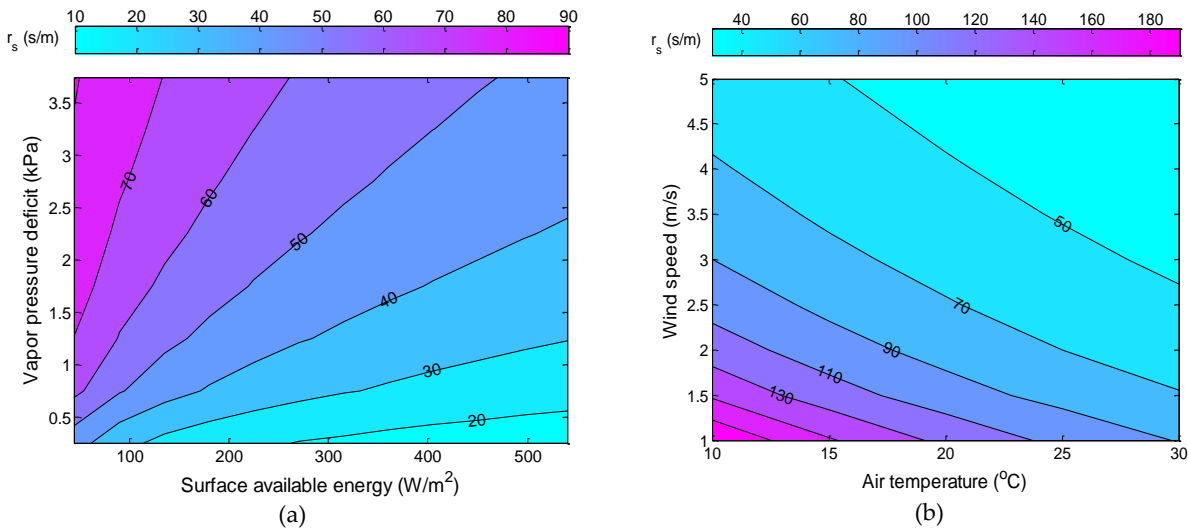
335 Before evaluating the performance of the constant  $EF_r$  method in upscaling instantaneous  
336 ET, the daytime variation in the half-hourly surface resistance estimated by Todorovic's method  
337 is examined in Figure 2. These daytime surface resistances were averaged over the days that had  
338 clear skies at 12:00-13:00 local time for the wheat and corn growth stages at the Yucheng and  
339 Yingke sites. Figure 2 clearly shows that the daytime surface resistance estimated from Eq. (1)  
340 exhibits a concave shape with the minimum occurring at noon and the maximum in the early  
341 morning or late afternoon. The averaged daytime surface resistance for the wheat (short crop)  
342 growth period was higher than that for the corn (tall crop) growth period at both sites. For both  
343 the wheat and corn growth periods, the estimated daytime surface resistance at the Yucheng site  
344 was between the fixed values recommended by the FAO-PM (70 s/m for short grass and 45 s/m  
345 for tall alfalfa) and the ASCE-PM (50 s/m for short grass and 30 s/m for tall alfalfa) equations  
346 near noon time (10:00 h - 14:00 h) but was higher than them in the early morning and late  
347 afternoon. At the Yingke site, the variable surface resistance was higher than the fixed values  
348 recommended by the FAO-PM and the ASCE-PM equations.

349 The concave shape and site-to-site differences in the surface resistance are primarily  
350 determined by the daytime evolution of the meteorological variables of surface available energy,  
351 vapor pressure deficit, and wind speed at both sites; the sensitivity analysis presented in Figure 3  
352 shows that a high vapor pressure deficit, a low wind speed, a low surface available energy, and a  
353 low air temperature can all lead to a high surface resistance and vice versa. Moreover, the  
354 sensitivity of the surface resistance to the surface available energy (wind speed, air temperature)

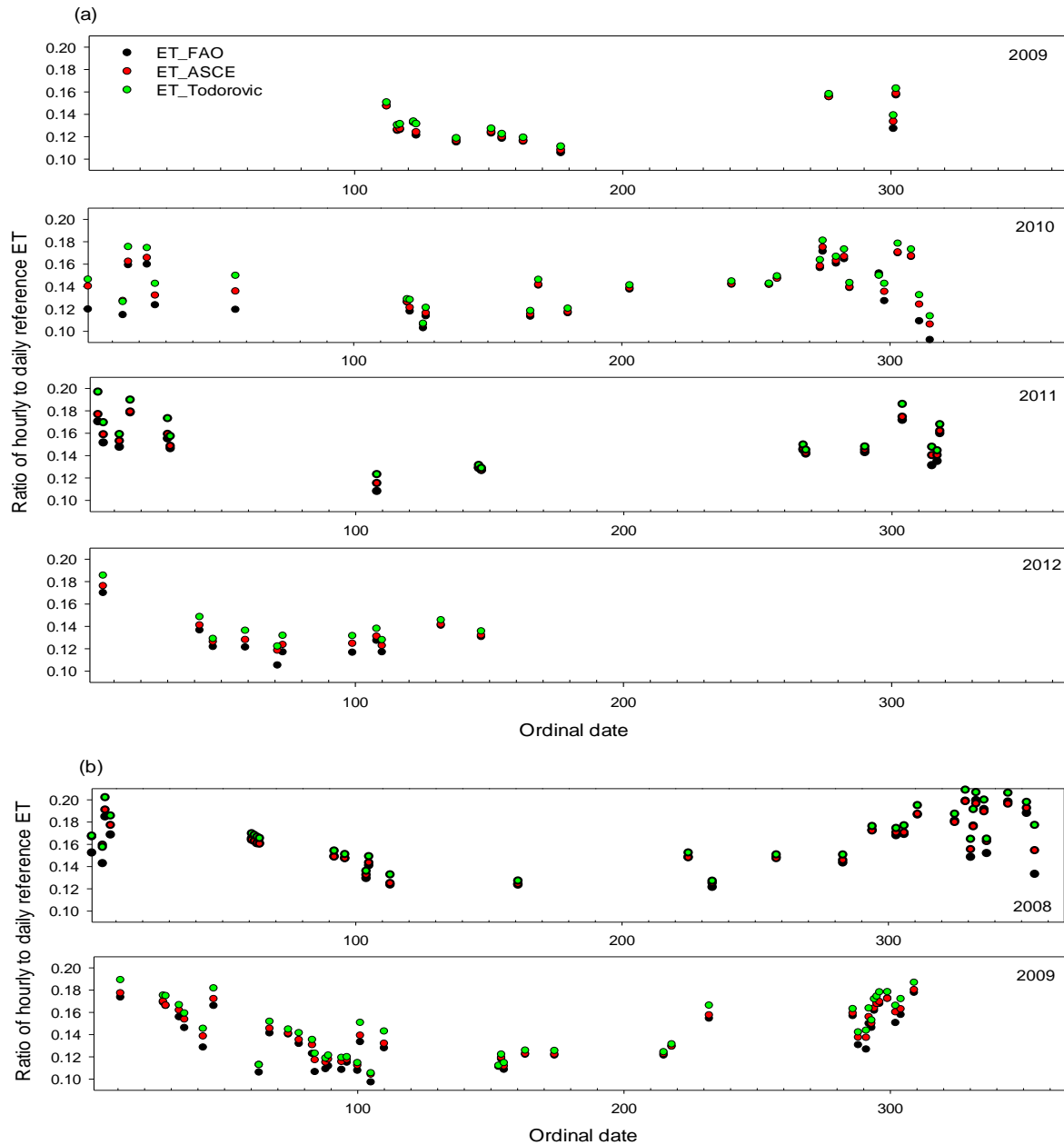
355 decreases when the surface available energy (wind speed, air temperature) increases, and a  
 356 higher sensitivity can be obtained with a higher vapor pressure deficit.



357  
 358 **Figure 2.** Daytime variations of half-hourly surface resistances estimated from the method  
 359 proposed by *Todorovic* [1999] and averaged over the selected days that have clear skies at 12:00-  
 360 13:00 local time for the wheat and corn growth stages at the Yucheng and Yingke sites.



361 **Figure 3. (a)** Contour of *Todorovic*'s variable surface resistance ( $r_s$ ) with the variations of  
 362 surface available energy and vapor pressure deficit, when air temperature is at 30 °C and wind  
 363 speed equals 3.0 m/s. **(b)** Contour of the  $r_s$  with the variations of air temperature and wind speed,  
 364 when surface available energy is at 450 W/m<sup>2</sup> and vapor pressure deficit equals 3.0 kPa.



365

366

367

368

369

370

371

372

373

374

375

376

377

378

**Figure 4.** Temporal variation of the ratios of 12:00-13:00 local time hourly to daily latent heat flux estimated from the FAO-PM, the ASCE-PM, and the full-form PM equations over the selected days at (a) Yucheng site from year 2009 to 2012 and (b) Yingke site from year 2008 to 2009.

Using fixed and variable surface resistances results in different daytime half-hourly reference ET estimates and, consequently, influences the ratio of the reference instantaneous ET to the daily ET. Using the noon data as an example, Figure 4a-b illustrates how the ratios of the hourly to daily reference ETs ( $ET_{r,h}/ET_{r,d}$ ) estimated from the FAO-PM, ASCE-PM, and full-form PM equations vary seasonally over the selected 68 days from April 2009 to June 2012 at the Yucheng site and over the selected 73 days from January 2008 to November 2009 at the Yingke site.

379 Overall, the  $ET_{r,h}/ET_{r,d}$  computed at 12:00-13:00 local time from the three PM equations  
380 showed similar seasonal patterns and magnitudes at both sites; higher values occur in the winter  
381 and lower values occur in the summer, which reflects the temporal variations in the vapor  
382 pressure deficit, the surface available energy, and the disparate percentage of noon-time ET in  
383 the daily ET in a yearly cycle. In most cases, the  $ET_{r,h}/ET_{r,d}$  ratio varied between  $\sim 0.1$  and  $\sim 0.2$  at  
384 both sites and was higher at the arid Yingke site than at the sub-humid Yucheng site. The  
385  $ET_{r,h}/ET_{r,d}$  using the full-form PM equation was generally higher than that using the ASCE-PM  
386 equation. Both were higher than that using the FAO-PM equation.

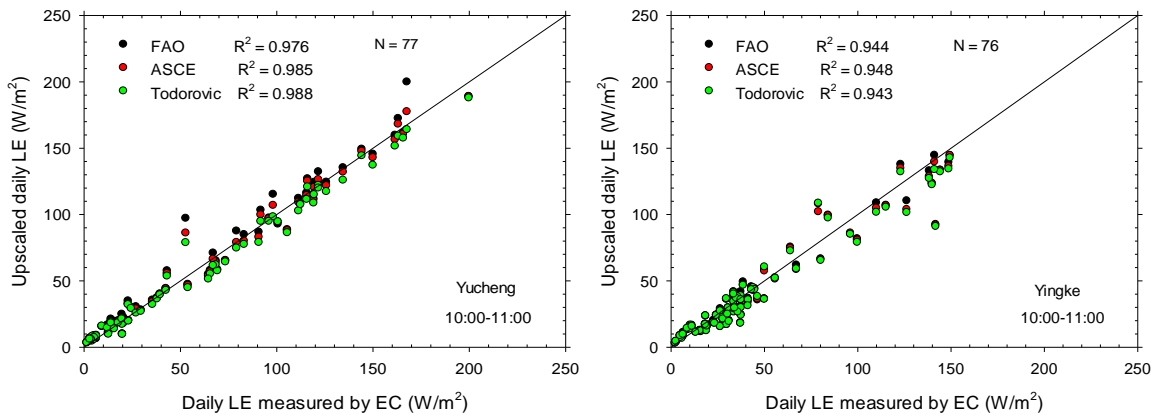
387 The discrepancy between the  $ET_{r,h}/ET_{r,d}$  ratios estimated using the variable and fixed  
388 surface resistances was larger when the ET was small and smaller when the ET was large, which  
389 indicates that using these three surface resistances and PM equations in the constant  $EF_r$  method  
390 would yield a larger relative difference in the upscaled daily ET in the winter than that in the  
391 summer. However, at both sites, the discrepancy between the  $ET_{r,h}/ET_{r,d}$  ratios in the wheat  
392 growth stage with short grass as the reference crop was not significantly different from that in the  
393 corn growth stage with tall alfalfa as the reference crop.

#### 394 4.2 Evaluation using original flux tower measurements

395 For a given time period, the paired-t test was used to test the null hypothesis that the mean of  
396 one PM model-predicted daily ET equals the mean of another PM model-predicted daily ET  
397 against the alternative hypothesis that the two statistics are not equal. After further selecting the  
398 days that had two assumed time periods, the paired-t test was separately used for all three PM  
399 equations to test the null hypothesis that the mean of the model-predicted ET at one time equals  
400 that at another time against the alternative hypothesis that the two statistics are not equal. The  
401 level of significance chosen for all tests was 0.05 (95% confidence level).

402 Figure 5a-f compares the daily ET measured by the EC without an energy correction and  
403 that ( $ET_{FAO-PM}$ ,  $ET_{ASCE-PM}$ , and  $ET_{TOD-PM}$ ) upscaled from the constant  $EF_r$  method, with the  
404 reference ET derived using the FAO-PM equation, the ASCE-PM equation, and the full-form  
405 PM equation at the Yucheng and Yingke sites. The corresponding statistical measures of the  
406 performance are illustrated in Figure 6a-c. (i) Using the three PM equations produced  
407 significantly different upscaled daily LEs at a given time from mid-morning to mid-afternoon,  
408 with an exception occurring at the Yingke site in the mid-morning between using the ASCE-PM  
409 equation and the full-form PM equation. (ii) At the Yucheng site, using the ASCE-PM equation  
410 and the full-form PM equation overall produced the best results from mid-morning to noon and  
411 in the mid-afternoon, respectively. Using the FAO-PM equation produced the worst results for  
412 all time intervals. At the Yingke site, using the FAO-PM equation and the full-form PM equation  
413 produced the best and the worst results, respectively, from mid-morning to noon whereas the  
414 opposite results were obtained in the mid-afternoon. (iii) Using all three PM equations tended to  
415 produce progressively larger upscaled daily LE from mid-morning to mid-afternoon. For a given  
416 time,  $ET_{FAO-PM} > ET_{ASCE-PM} > ET_{TOD-PM}$ . (iv) For all three PM equations, the daily LE upscaled in  
417 the mid-morning was not significantly different from that in the noon time, and the model  
418 performances were overall statistically better in the mid-morning and noon time than those in the  
419 mid-afternoon.

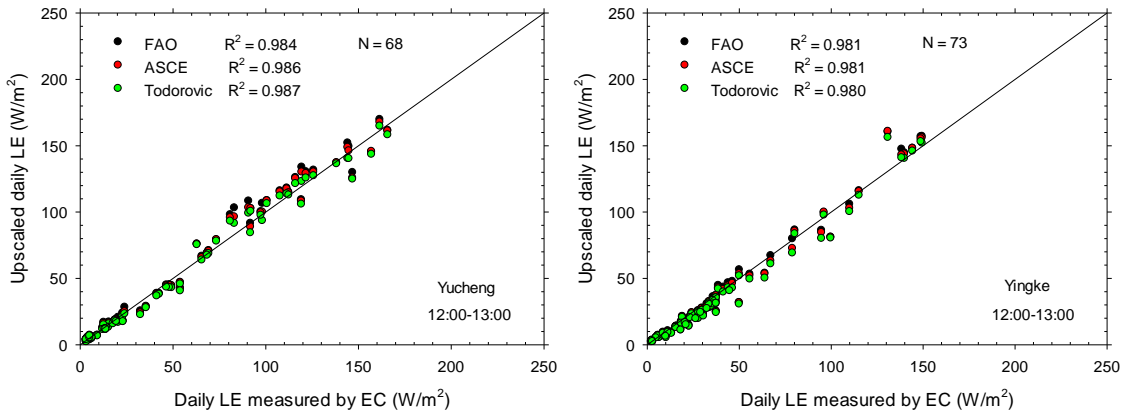
420



421  
422

(a)

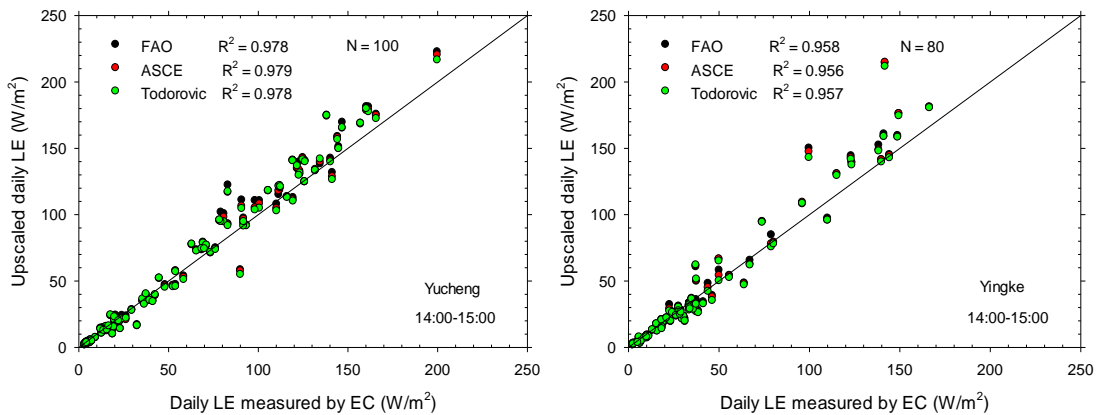
(b)



423  
424

(c)

(d)



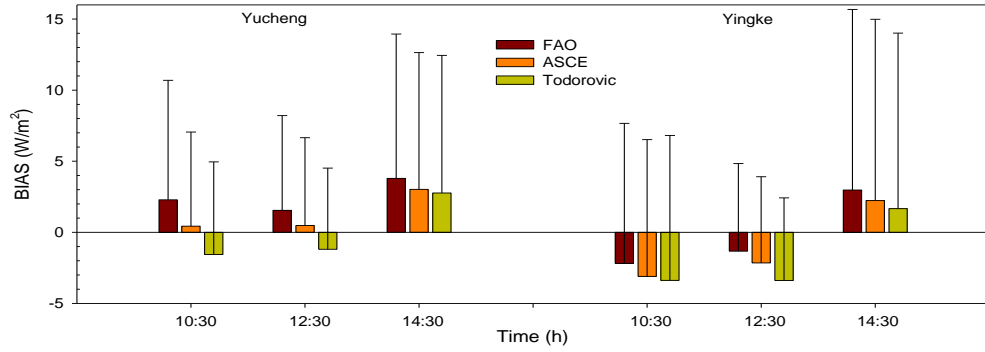
425  
426

(e)

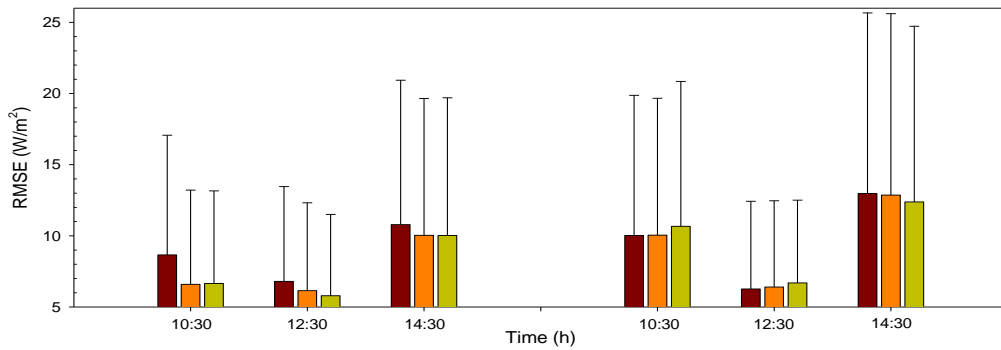
(f)

**Figure 5.** Comparison of the daily LE measured by eddy covariance system without an energy correction with that derived by the constant reference evaporative fraction method at three different local time periods in the daytime over selected clear skies. (a), (c), and (e) for the Yucheng site, (b), (d), and (f) for the Yingke site.

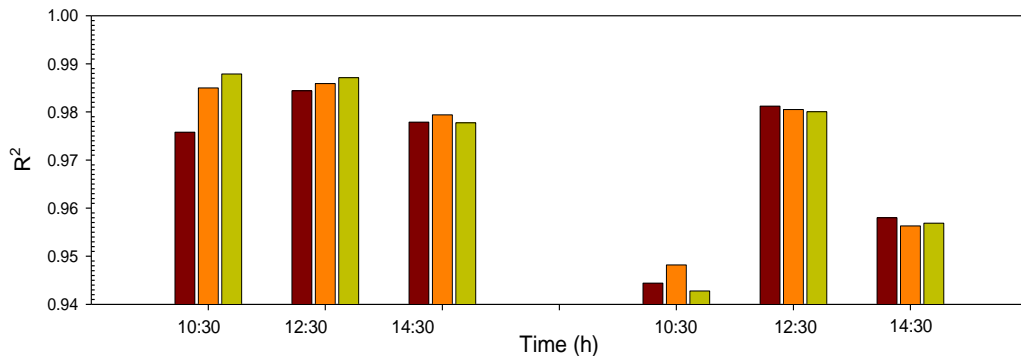
431



(a)



(b)



(c)

**Figure 6.** Statistical measures of the performance of constant reference evaporative fraction upscaling method in converting hourly ET estimated using the FAO-PM, the ASCE-PM, and the full-form PM equations at different clear sky time periods in the daytime to daily value over selected days (10:30 stands for 10:00-11:00 interval, similarly hereafter). The error bar represents one standard deviation of the difference between model-estimated and EC-measured daily ETs. For each of the panels, the left part is for the Yucheng site and the right part is for the Yingke site. The EC-measured LE was not corrected to close the energy imbalance. **(a)** BIAS, **(b)** root mean square error (RMSE), **(c)** coefficient of determination ( $R^2$ ).

#### 4.3 Evaluation using corrected flux tower measurements

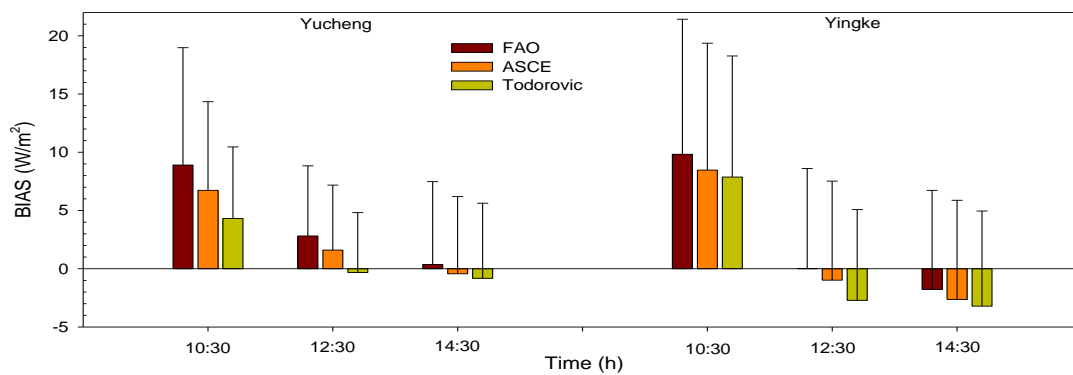
The energy closure ratio, which is defined as the ratio of the sum of the half-hourly EC-measured H and LE to the surface available energy, for the quality-, completeness-, and relative

450 humidity-controlled days averaged 0.81 and 0.67 at the Yucheng and the Yingke sites,  
451 respectively. The paired-t test that was used in Section 4.2 was also applied in this section to  
452 evaluate the significance of the statistical results.

453 Figure 7a-c shows the statistical measures of the performance of the constant  $EF_r$  upscaling  
454 method after using the BR correction method introduced in Section 3.3 to close the energy  
455 imbalance of the original EC measurements. At the Yucheng site, different from the results  
456 without the correction of surface energy imbalance, using the full-form PM equation and the  
457 FAO-PM equation produced the best and the worst results, respectively, from mid-morning to  
458 noon, whereas the opposite results were obtained in the mid-afternoon. At the Yingke site, using  
459 the three PM equations produced significantly different upscaled daily LEs at a given time from  
460 mid-morning to mid-afternoon with no exceptions. Using the FAO-PM equation and the full-  
461 form PM equation produced the best and worst results, respectively, from noon to mid-afternoon,  
462 whereas the opposite results were obtained in the mid-morning. Moreover, at both sites, using all  
463 three PM equations tended to produce progressively smaller upscaled daily LEs from mid-  
464 morning to mid-afternoon. For a given PM equation, the daily LE upscaled at one time was  
465 significantly different from that at another time from mid-morning to mid-afternoon (with an  
466 exception at the Yingke site for the full-form PM equation between noon time and mid-  
467 afternoon) and the best model performance tended to occur in the noon time.

468 Figure 8a-c shows the statistical measures of the performance of the constant  $EF_r$  upscaling  
469 method when using the RE correction method to close the energy imbalance of the original EC  
470 measurements. At the Yucheng site, the results were completely the same as those obtained when  
471 the BR correction method was applied. At the Yingke site, the results were almost the same as  
472 those obtained using the BR correction method. The only difference was that the daily LE  
473 upscaled at one time for a given PM equation was significantly different from that at another  
474 time from mid-morning to mid-afternoon with no exceptions.

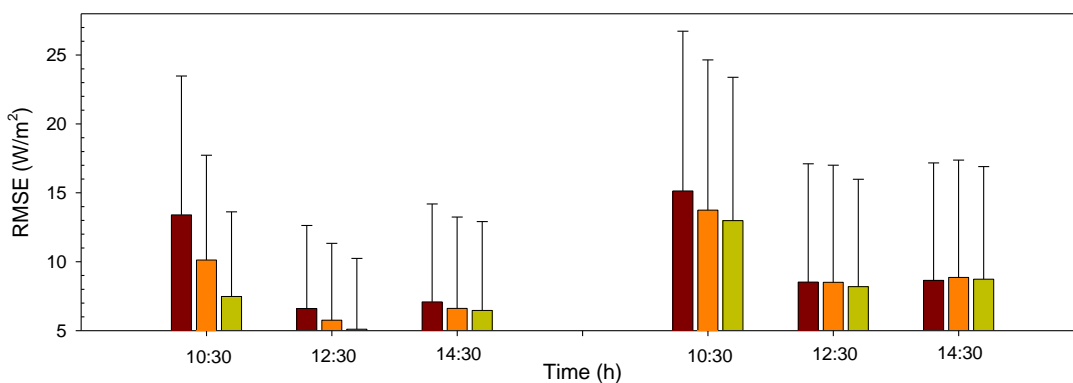
475



476

477

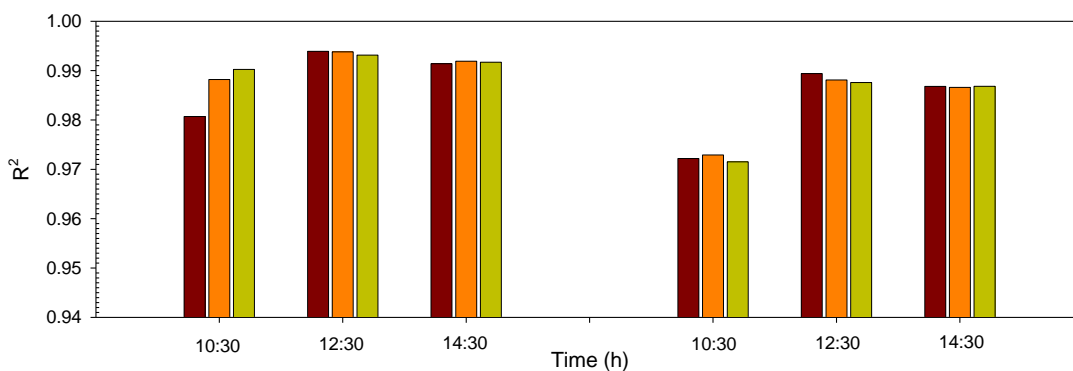
(a)



478

479

(b)



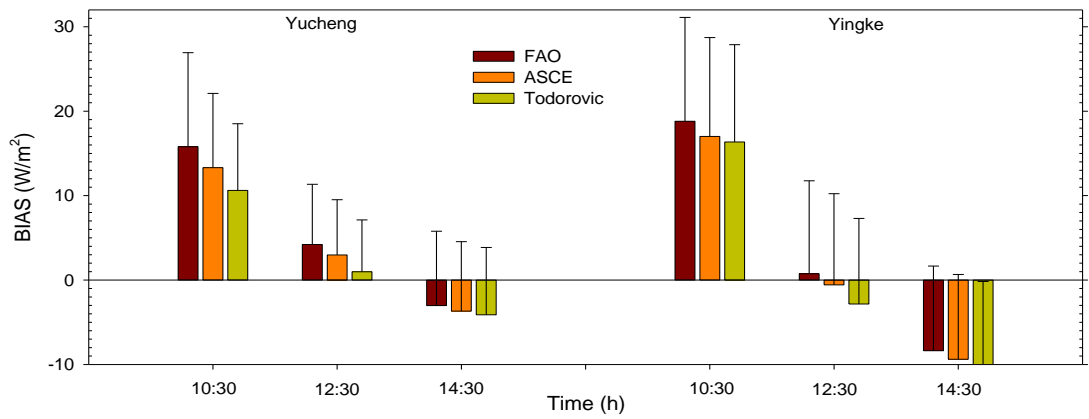
480

481

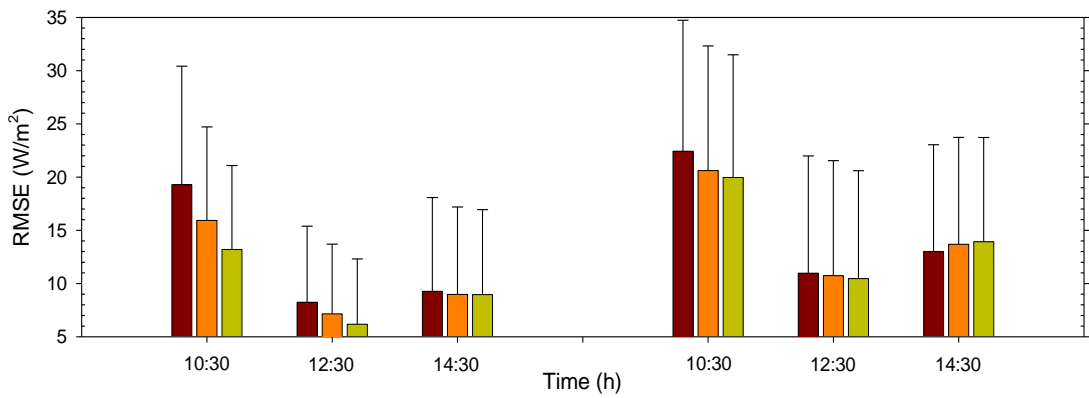
(c)

482 **Figure 7.** Comparison of Same as Figure 6, but for the application of energy closure of the EC-  
483 measured LE using the Bowen ratio correction method.

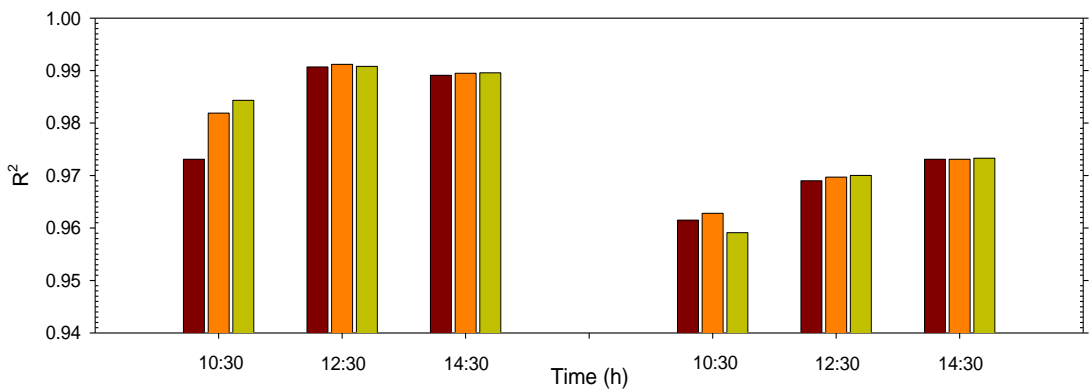
484



(a)



(b)



(c)

**Figure 8.** Same as Figure 6, but for the application of energy closure of the EC-measured LE using the residual energy correction method.

485  
486

487  
488

489  
490  
491  
492  
493

494 4.4 Discussion

495 The performance of the constant  $EF_r$  upscaling method in practical applications depends on  
496 how close the instantaneous  $EF_r$  at a given clear-sky satellite overpass time is to the daily  
497 average. When the instantaneous  $EF_r$  is larger (or smaller) than the daily average, the upscaled  
498 daily LE will be overestimated (or underestimated). Using the constant  $EF_r$  method to upscale  
499 the LE requires accurate estimates of the reference hourly and daily ET values.

500 Given the same magnitude of the decrease in the surface resistance for all of the hourly  
501 periods during the daytime, the relative increase in the hourly reference ET from mid-morning to  
502 mid-afternoon is generally larger than that in the early morning and late afternoon because the  
503 reference ET near midday accounts for the largest fraction of the daily average. Due to the  
504 combined effect of the reduced nighttime reference ET and the smaller increase in the early  
505 morning and late-afternoon reference ET values than the mid-morning to mid-afternoon  
506 reference ET values, the relative increase in the hourly reference ET from mid-morning to mid-  
507 afternoon will generally be greater than the relative increase in the daily average, which results in  
508 a larger  $ET_{r,h}/ET_{r,d}$  and a smaller upscaled daily LE when using the ASCE-PM equation than  
509 when using the FAO-PM equation. In contrast, using the greater variable surface resistances  
510 derived from Todorovic's method than the fixed values adopted in the ASCE-PM equation  
511 produced smaller daytime reference ET estimates and, consequently, smaller daily reference ET  
512 estimates. Because the variable surface resistance has a concave shape during the daytime, the  
513 relative decrease in the hourly reference ET has a convex shape, and its absolute value is  
514 significantly smaller in the midday period than in the early morning and late afternoon. This  
515 most likely produces a larger  $ET_{r,h}/ET_{r,d}$  in the full-form PM equation than that in the ASCE-PM  
516 equation and a smaller upscaled daily LE. The large standard deviation as shown in Figures 6-8  
517 may indicate the instability of the  $EF_r$  in a diurnal cycle under some circumstances over the wide  
518 range of atmospheric and soil moisture conditions at both sites (in other words, using the  
519 constant  $EF_r$  upscaling method can create a large bias in the daily ET).

520 Progressively smaller upscaled daily ET values from mid-morning to mid-afternoon using  
521 the constant  $EF_r$  method have also been found in previous studies [*Cammalleri et al.*, 2014; *Tang*  
522 *et al.*, 2013a]. When the upscaled daily ET values from the constant  $EF_r$  method were compared  
523 to the EC measurements without an energy imbalance correction, the overestimation (positive  
524 bias) during the mid-morning and underestimation (negative bias) during the mid-afternoon in  
525 this study and our prior study [*Tang et al.*, 2013a] were not consistent with the results of  
526 *Cammalleri et al.* [2014], who found a stable underestimation in the upscaled daytime ET from  
527 mid-morning to mid-afternoon. Our finding that the noon time overall appeared to be the optimal  
528 time for instantaneous ET upscaling has also been revealed by other researchers [*Colaizzi et al.*,  
529 2006; *Delogu et al.*, 2012; *Tang et al.*, 2013a; *Cammalleri et al.*, 2014]. Because the  $ET_{r,h}/ET_{r,d}$   
530 does not vary before and after the energy imbalance correction, how the model performance of a  
531 given PM equation changes with the energy closure at a given time entirely depends on the  
532 relative variation in the corrected hourly and daily EC-measured ET. This may also lead to a  
533 change in the same inter-model performances of the three PM equations. Site-to-site and time-to-  
534 time variations were found in this study in the performances of a given PM equation before and  
535 after the energy imbalance was closed, which agreed with *Cammalleri et al.* [2014] and *Tang et*  
536 *al.* [2013a], who found that the closure of EC measurements could have a significant effect on  
537 the choice of optimal upscaling technique. Because no studies have ever attempted to incorporate  
538 a variable daytime surface resistance in the upscaling of instantaneous ET data using the constant  
539  $EF_r$  method, our findings that are associated with the best upscaling technique and the optimal

540 upscaling time in the three PM equations in this study cannot be further corroborated by the work  
541 of other authors.

542 Unexpectedly, using variable surface resistances did not produce a much closer upscaled  
543 daily ET to using a fixed surface resistance as adopted in the ASCE-PM equation at the sub-  
544 humid Yucheng site than at the arid Yingke site. This may be because the reference ET estimate  
545 is controlled not by the absolute value of the surface resistance but primarily by the ratio of the  
546 surface to aerodynamic resistances; both resistances generally have similar diurnal patterns.  
547 Underestimated daily LE values upscaled from the constant  $EF_r$  method at 12:00-13:00 local  
548 time using Todorovic's variable surface resistance in the reference ET estimates at the arid site in  
549 this study are also found in the work of *Liu et al.* [2012] when the BR correction method is  
550 applied to close the energy imbalance of the EC measurements. Both studies produced relative  
551 root mean square errors (RMSEs, ratio of the RMSE to the observed mean) with similar  
552 magnitudes. However, the constant  $EF_r$  method using Todorovic's variable surface resistance  
553 performs better at the humid Yucheng site than at the arid Yingke site, with lower (relative)  
554 absolute BIAS and RMSE values but a higher coefficient of determination ( $R^2$ ). This may be  
555 explained by the explanation by *Allen et al.* [2006] that the climatic resistance model of  
556 Todorovic works reasonably well for rain-fed agriculture but can fail in irrigated areas in semi-  
557 arid and arid climates. Based on studies by European and American researchers, *Allen et al.*  
558 [2006] recommended using fixed surface resistance values of 50 s/m for daytime and 200 s/m for  
559 nighttime for the reference ET estimates. Nevertheless, several authors have demonstrated that  
560 using variable surface resistances is preferential to using a fixed surface resistance of 70 m/s for  
561 daytime reference ET estimates, even at semi-arid sites [*Todorovic*, 1999; *Lecina et al.*, 2003;  
562 *Perez et al.*, 2006]. Moreover, using variable surface resistances in this study was indeed able to  
563 produce better daily ET estimates in the constant  $EF_r$  upscaling method in the mid-afternoon  
564 compared to using fixed surface resistances at both the Yucheng and Yingke sites when the  
565 energy imbalance of the EC measurements was not closed.

566 The low energy closure ratio (0.67 at the Yingke site) or the surface energy imbalance can  
567 be caused by a number of other factors [*Wilson et al.*, 2002; *Foken*, 2008; *Stoy et al.*, 2013],  
568 among which include the measurement errors of surface energy components, the mismatch of  
569 source areas between surface flux components, the uncorrection of heat storage for  $G$ , the neglect  
570 of the heat storage in the canopy, the neglect of photosynthetic and advective energy, and the  
571 dispersive fluxes not sampled by the EC system. The reasons for the closure errors in the EC  
572 measurements are difficult to realistically identify because so many factors can influence the  
573 energy imbalance. These various influencing factors and the applied correction methods can  
574 have an impact on the EC-measured ET and the validation results of upscaled daily ET. The  
575 error in the validation of upscaled daily ET is therefore difficult to attribute to a certain factor  
576 (e.g., poor  $G$  representation) or a correction method. Nevertheless, knowledge of the model  
577 performances under given conditions at the Yucheng and Yingke sites is still valuable.

578 The limitation in using the constant  $EF_r$  upscaling method primarily lies in its requirement  
579 of metrological measurements (solar radiation, air temperature, vapor pressure deficit, wind  
580 speed) as inputs. However, a great advantage of using this method towards other simpler scaling  
581 techniques (e.g., using at-surface solar radiation as the reference variable, as in *Cammalleri et al.*  
582 [2014] and using surface net radiation as the reference variable, as in *Nagler et al.* [2009]) is that  
583 it can incorporate the effect of advective energy and time-dependent environmental variables on  
584 the ET in a diurnal cycle. Moreover, deriving a variable resistance does not require inputs any  
585 more than estimating the reference ET from the Penman-Monteith equation when the constant

586  $E_{Fr}$  upscaling method is applied. Using variable surface resistance could potentially improve the  
587 reference ET estimates and thus the ET upscaling in the constant  $E_{Fr}$  method [Liu *et al.*, 2012;  
588 Pereira *et al.*, 1999; Rana and Katerji, 2000; Lecina *et al.*, 2013; Perez *et al.*, 2006].

## 589 **5 Summary and conclusions**

590 In the upscaling of instantaneous ET, both the constant  $E_{Fr}$  method and the constant global  
591 solar radiation ratio method outperform the constant evaporative fraction method, the constant  
592 extraterrestrial solar radiation ratio method, and the sinusoidal function method, though there is  
593 no agreement on which of the former two methods performs better [Xu *et al.*, 2015; Tang *et al.*,  
594 2013; Cammalleri *et al.*, 2014]. To investigate whether the use of a variable surface resistance in  
595 the reference ET estimation from the PM equation, as proposed by Todorovic [1999], can  
596 improve the daily upscaled ET on clear-sky days from the constant  $E_{Fr}$  method, half-hourly near-  
597 surface meteorological variables and EC-measured LE values were collected as the model inputs  
598 and validation data, respectively, at two sites with contrasting climatic conditions, namely, the  
599 sub-humid Yucheng station in northern China and the arid Yingke site in northwestern China.  
600 The use of Todorovic's variable surface resistance in this study does not require a priori  
601 calibration.

602 The results before the energy imbalance in the EC measurements was closed are  
603 summarized as follows:

- 604 i) In the mid-afternoon, using variable surface resistance in the full-form PM equation at both  
605 sites produced the best ET upscaling results, and using fixed resistance in the FAO-PM  
606 equation produced the worst results.
- 607 ii) In the mid-morning to noon, using fixed resistance in the ASCE-PM equation at the  
608 Yucheng site produced the best results, and using the FAO-PM equation produced the  
609 worst results. At the Yingke site, using the FAO-PM equation and the full-form PM  
610 equation produced the best and worst results, respectively.
- 611 iii) For all three PM equations, the daily LE upscaled in the mid-morning was not significantly  
612 different from that in the noon time, and the model performances were overall statistically  
613 better in the mid-morning and noon time than in the afternoon.
- 614 iv) At both sites, using all three PM equations tended to produce progressively larger upscaled  
615 daily LEs from mid-morning to mid-afternoon. For a given time,  $ET_{FAO-PM} > ET_{ASCE-PM} >$   
616  $ET_{TOD-PM}$ .

617 After the energy imbalance was closed using the BR and RE correction methods, some  
618 changes were found in the results as follows:

- 619 i) In the mid-morning, using the full-form PM equation at both sites produced the best  
620 results, and using fixed resistance in the FAO-PM equation produced the worst results.
- 621 ii) In the mid-afternoon, using the FAO-PM equation and the full-form PM equation at the  
622 Yucheng site produced the best and the worst results, respectively. The opposite results  
623 were obtained at the Yingke site.
- 624 iii) In the noon time, using the full-form PM equation at the Yucheng site produced the best  
625 results, and using the FAO-PM equation produced the worst results. The opposite results  
626 were obtained at the Yingke site.
- 627 iv) For a given PM equation, the daily LE upscaled at one time was significantly different  
628 from that at another time from mid-morning to mid-afternoon, and the best model  
629 performance tended to occur in the noon time.

630 v) At both sites, using all three PM equations tended to produce progressively smaller  
631 upscaled daily LEs from mid-morning to mid-afternoon.

632 In summary, using the three PM equations produced significantly different upscaled daily  
633 ETs ( $ET_{FAO-PM} > ET_{ASCE-PM} > ET_{TOD-PM}$ ) at a given time from mid-morning to mid-afternoon.  
634 Using all three PM equations overall produced the best results at noon at both sites regardless of  
635 whether the energy imbalance was closed. When the EC measurements were not corrected for  
636 energy imbalance, using variable surface resistance in the full-form PM equation could improve  
637 the ET upscaling in the mid-afternoon, but worse results may occur in the mid-morning to noon.  
638 Site-to-site and time-to-time variations were found in the performances of a given PM equation  
639 before and after the energy imbalance was closed. At a given site, using the BR correction  
640 method yields the same inter-model performances for the three PM equations as using the RE  
641 correction method. It has to be mentioned that when detailed meteorological measurements are  
642 not available at the ground station, to temporally upscale the remote sensing instantaneous ET in  
643 a practical application using the constant  $EF_r$  method, regional reference ET can be estimated  
644 with reanalysis data from numerical weather prediction models and global climate models (Tian  
645 and Martinez 2012; Ishak et al. 2010). When soil heat flux measurement is not available, to close  
646 the energy imbalance of EC measurements, semi-empirical relationships as proposed by Kustas  
647 and Daughtry (1990), Bastiaanssen et al. (1998), and Su (2002) can be applied to derive a  
648 spatially representative soil heat flux from surface net radiation measurement and remote sensing  
649 vegetation index. Note that although the evaluation in this study is only conducted at two sites, it  
650 is instructive and can be conclusive to a great extent because these two sites are characterized by  
651 contrasting climatic conditions and data involved cover a wide range of soil moisture and  
652 vegetation cover conditions. To make a general conclusion, more extensive assessments and  
653 validations are required over a wider range of climate, soil moisture, and plant functional type  
654 conditions.

## 655 **Acknowledgments and Data**

656 The staff members at the Yucheng site are acknowledged for their hard-work on the setup  
657 and maintenance of the ground-based instruments and data collection. Associate Professor  
658 Yuanyuan Jia and Professor Chuanrong Li in the Academy of Opto-Electronics, Chinese  
659 Academy of Sciences, are thanked for their cooperation in providing the surface measurements.  
660 EC data at the Yingke site used in this study are downloaded from “Environmental & Ecological  
661 Science Data Center for West China, National Natural Science Foundation of China,  
662 <http://westdc.westgis.ac.cn>”. This work was partly supported by the National Natural Science  
663 Foundation of China under Grant 41571351 and 41571367, and in part by the International  
664 Science and Technology Cooperation Program of China under Grant 2014DFE10220.

## 665 **References**

- 666 Allen, R. G., L. S. Pereira, D. Raes, and M. Smith (1998), Crop evapotranspiration-Guidelines  
667 for computing crop water requirements, FAO Technical Paper 56, Food and Agricultural  
668 Organization of the United Nations, Rome, 300(9), D05109.
- 669 Allen, R. G., W. O. Pruitt, J. L. Wright, T. A. Howell, F. Ventura, R. Snyder, D. Itenfisu, P.  
670 Steduto, J. Berengena, J. Yrisarry, M. Smith, L. Pereira, D. Raes, A. Perrier, I. Alves, I.  
671 Walter, and R. Elliott (2006), A recommendation on standardized surface resistance for

672 hourly calculation of reference ETo by the FAO56 Penman-Monteith method, *Agr. Water*  
673 *Manage.*, 81(1), 1-22, doi:10.1016/j.agwat.2005.03.007.

674 Allen, R. G., M. Tasumi, and R. Trezza (2007), Satellite-based energy balance for mapping  
675 evapotranspiration with internalized calibration (METRIC)-model, *J Irrig. Drain. E.*,  
676 133(4), 380–394, doi: 10.1061/(ASCE)0733-9437(2007)133:4(380).

677 Alves, I., and L. S. Pereira (2000), Modelling surface resistance from climatic variables?, *Agr.*  
678 *Water Manage.*, 42(3), 371-385, doi: 10.1016/S0378-3774(99)00041-4.

679 ASCE-EWRI. (2005), The ASCE Standardized Reference Evapotranspiration Equation.  
680 Technical Committee report to the Environmental and Water Resources Institute of the  
681 American Society of Civil Engineers from the Task Committee on Standardization of  
682 Reference Evapotranspiration, ASCE-EWRI, 1801 Alexander Bell Drive, Reston, VA  
683 20191-4400, 173 pp, doi:10.1061/40499(2000)126.

684 Baldocchi, D., E. Falge, L. Gu, R. Olson, D. Hollinger, S. Running, P. Anthoni, C. Bernhofer, K.  
685 Davis, R. Evans, J. Fuentes, A. Goldstein, G. Katul, B. Law, X. Lee, Y. Malhi, T.  
686 Meyers, W. Munger, W. Oechel, K. Paw, K. Pilegaard, H. Schmid, R. Valentini, S.  
687 Verma, T. Vesala, K. Wilson, and S. Wofsy (2001), FLUXNET: A new tool to study the  
688 temporal and spatial variability of ecosystem-scale carbon dioxide, water vapor, and  
689 energy flux densities, *B. AM. Meteorol. Soc.*, 11, 2415-2434, doi:10.1175/1520-  
690 0477(2001)082<2415:FANTTS>2.3.CO.

691 Bastiaanssen, W. G. M., M. Menenti, R. A. Feddes, and A. A. M. Holtslag (1998), A remote  
692 sensing surface energy balance algorithm for land (SEBAL). 1. Formulation, *J. Hydrol.*,  
693 212, 198-212, doi:10.1016/S0022-1694(98)00254-6.

694 Brutsaert, W., and M. Sugita (1992), Application of self-preservation in the diurnal evolution of  
695 the surface energy budget to determine daily evaporation, *J. Geophys. Res.*, 97, 18377-  
696 18382, doi:10.1029/92JD00255.

697 Burba, G., and D. Anderson (2010), A brief practical guide to eddy covariance flux  
698 measurements: principles and workflow examples for scientific and industrial  
699 applications, LI-COR Biosciences, Lincoln, Nebraska, USA, 212 pp,  
700 doi:10.13140/RG.2.1.1626.4161.

701 Cammalleri, C., M. C. Anderson, and W. P. Kustas (2014), Upscaling of evapotranspiration  
702 fluxes from instantaneous to daytime scales for thermal remote sensing applications,  
703 *Hydrol. Earth Syst. Sc.*, 18, 1885-1894, doi:10.5194/hess-18-1885-2014.

704 Chávez, J. L., C. M. Neale, J. H. Prueger, and W. P. Kustas (2008), Daily evapotranspiration  
705 estimates from extrapolating instantaneous airborne remote sensing ET values, *Irrigation.*  
706 *Sc.*, 27, 67-81, doi:10.1007/s00271-008-0122-3.

707 Colaizzi, P. D., S. R. Evett, T. A. Howell, and J. A. Tolk (2006), Comparison of five models to  
708 scale daily evapotranspiration from one-time-of-day measurements, *T. ASAE.*, 49, 1409-  
709 1417, doi:10.13031/2013.22056.

710 Delogu, E., G. Boulet, A. Olioso, B. Coudert, j. Chirouze, E. Ceschi, B. Le Dantec, O. Marloie,  
711 G. Chehbouni, and J.-P. Lagouarde (2012), Reconstruction of temporal variations of  
712 evapotranspiration using instantaneous estimates at the time of satellite overpass, *Hydrol.*  
713 *Earth Syst. Sc.*, 16, 2995-3010, doi:10.5194/hess-16-2995-2012.

- 714 Foken, T. (2008). The energy balance closure problem: An overview, *Ecol. Appl.*, *18*, 1351-  
715 1367, doi:10.1890/06-0922.1.
- 716 Jackson, R. D., J. L. Hatfield, R. J. Reginato, S. B. Idso, and P. Pinter (1983), Estimation of daily  
717 evapotranspiration from one time of day measurements, *Agr. Water Manage.*, *7*, 351-362,  
718 doi:10.1016/0378-3774(83)90095-1.
- 719 Ishak, A. M., M. Bray, R. Remesan, and D. Han (2010), Estimating reference evapotranspiration  
720 using numerical weather modelling, *Hydrol. Process.*, *24*(24), 3490–3509,  
721 doi:10.1002/hyp.7770.
- 722 Jia, L., G. Xi, S. Liu, C. Huang, Y. Yan, and G. Liu (2007), Regional estimation of daily to  
723 annual regional evapotranspiration with MODIS data in the Yellow River Delta wetland,  
724 *Hydrol. Earth Syst. Sci.*, *13*, 1775–1787, doi:10.5194/hessd-6-2301-2009.
- 725 Kalma, J. D., T. R. McVicar, and M. F. McCabe (2008), Estimating land surface evaporation: a  
726 review of methods using remotely sensed surface temperature data, *Surv. Geophys.*, *29*,  
727 421–469, doi:10.1007/s10712-008-9037-z.
- 728 Katerji, N., A. Perrier, D. Renard, and A. K. O. Aissa (1983), Modélisation de  
729 l'évapotranspiration réelle ETR d'une parcelle de luzerne: rôle d'un coefficient cultural,  
730 *Agronomie.*, *3*(6), 513-521, doi:10.1051/agro:19830603.
- 731 Kustas, W. P., and C. S. T. Daughtry (1990), Estimation of the soil heat flux/net radiation ratio  
732 from spectral data, *Agr. Forest Meteor.*, *49*, 205–223, doi:10.1016/0168-1923(90)90033-  
733 3.
- 734 Lecina, S., A. Martinez-Cob, P. J. Pérez, F. J. Villalobos, and J. J. Baselga (2003), Fixed versus  
735 variable bulk canopy resistance for reference evapotranspiration estimation using the  
736 Penman-Monteith equation under semiarid conditions, *Agr. Water Manage.*, *60*(3), 181-  
737 198, doi:10.1016/S0378-3774(02)00174-9.
- 738 Li, Z. -L., R. L. Tang, Z. Wan, Y. Bi, C. Zhou, B. Tang, G. Yan, and X. Zhang (2009), A Review  
739 of current methodologies for regional evapotranspiration estimation from remotely  
740 sensed data, *Sensors*, *9*, 3801–3853, doi:10.3390/s90503801.
- 741 Li, Z. -L., B. H. Tang, H. Wu, H. Ren, G. Yan, Z. Wan, I. F. Trigo, and J. A. Sobrino (2013a),  
742 Satellite-derived land surface temperature: Current status and perspectives, *Remote Sens.*  
743 *Environ.*, *131*, 14-37, doi:10.1016/j.rse.2012.12.008.
- 744 Li, Z. -L., H. Wu, N. Wang, S. Qiu, J. A. Sobrino, Z. Wan, B. Tang, and G. Yan (2013b), Land  
745 surface emissivity retrieval from satellite data, *Int. J. Remote Sens.*, *34*(9-10), 3084-3127,  
746 doi:10.1080/01431161.2012.716540.
- 747 Liu, G., M. Hafeez, Y. Liu, D. Xu, and C. Vote (2012), A novel method to convert daytime  
748 evapotranspiration into daily evapotranspiration based on variable canopy resistance, *J.*  
749 *Hydrol.*, *414*, 278-283, 10.1016/j.jhydrol.2011.10.042.
- 750 Liu, S. M., Z. W. Xu, W. Z. Wang, Z. Z. Jia, M. J. Zhu, J. Bai, and J. M. Wang (2011), A  
751 comparison of eddy-covariance and large aperture scintillometer measurements with  
752 respect to the energy balance closure problem, *Hydrol. Earth Syst. Sc.*, *15*(4), 1291-1306,  
753 doi:10.5194/hess-15-1291-2011.

- 754 Nagler, P. L., K. Morino, R. S. Murray, J. Osterberg, and E. P. Glenn (2009), An empirical  
755 algorithm for estimating agricultural and riparian evapotranspiration using MODIS  
756 enhanced vegetation index and ground measurements of ET. I. Description of method,  
757 *Remote Sens.*, *1*(4), 1273-1297, doi:10.3390/rs1041125.
- 758 Pereira, L. S., A. Perrier, R. G. Allen, and I. Alves (1999), Evapotranspiration: concepts and  
759 future trends, *J. Irrig. Drain. E.*, *125*(2), 45-51, doi:10.1061/(ASCE)0733-  
760 9437(1999)125:2(45).
- 761 Perez, P. J., S. Lecina, F. Castellvi, A. Martínez-Cob, and F. J. Villalobos (2006), A simple  
762 parameterization of bulk canopy resistance from climatic variables for estimating hourly  
763 evapotranspiration, *Hydrol. Process.*, *20*(3), 515-532, doi:10.1002/hyp.5919.
- 764 Rana, G., and N. Katerji (2000), Measurement and estimation of actual evapotranspiration in the  
765 field under Mediterranean climate: a review, *Eur. J. Agron.*, *13*(2), 125-153,  
766 doi:10.1016/S1161-0301(00)00070-8.
- 767 Ryu, Y., D. D. Baldocchi, T. A. Black, M. Detto, B. E. Law, R. Leuning, A. Miyata, M.  
768 Reichstein, R. Vargas, C. Ammann, J. Beringer, L. Flanagan, L. Gu, L. Hutley, J. Kim,  
769 H. McCaughey, E. Moors, S. Rambal, and T. Vesala (2012), On the temporal upscaling  
770 of evapotranspiration from instantaneous remote sensing measurements to 8-day mean  
771 daily-sums, *Agr. Forest Meteor.*, *152*, 212-222, doi:10.1016/j.agrformet.2011.09.010.
- 772 Shuttleworth, W. J., R. J. Gurney, A. Y. Hsu, and J. P. Ormsby (1989), FIFE: the variation in  
773 energy partition at surface flux sites, *Int. Assoc. Hydrol. Sc. Publ.*, *186*, 67-74.
- 774 Stoy, P. C., M. Mauder, T. Foken, B. Marcolla, E. Boegh, A. Ibrom, A. Arain, A. Arneth, M.  
775 Aurela, B. Bernhofer, A. Cescatti, E. Kellwik, P. Duce, D. Gianelle, E. Gorsel, G. Kiely,  
776 A. Knohl, H. Margolis, H. McCaughey, L. Merbold, L. Montagnani, D. Papale, M.  
777 Reichstein, M. Saunders, P. Serrana-Ortiz, M. Sottocornola, D. Spano, F. Vaccari, and A.  
778 Varlagin (2013), A data-driven analysis of energy balance closure across FLUXNET  
779 research sites: The role of landscape scale heterogeneity, *Agr. Forest Meteor.*, *171*, 137-  
780 152, doi:10.1016/j.agrformet.2012.11.004.
- 781 Su, Z. (2002), The surface energy balance system (SEBS) for estimation of turbulent heat fluxes,  
782 *Hydrol. Earth Syst. Sc.*, *6*, 85-99, doi:10.5194/hess-6-85-2002.
- 783 Sugita, M., and W. Brutsaert (1991), Daily evaporation over a region from lower boundary layer  
784 profiles measured with radiosondes, *Water Resour. Res.*, *27*, 747-752,  
785 doi:10.1029/90WR02706.
- 786 Sun, Z., Q. Wang, B. Matsushita, T. Fukushima, Z. Ouyang, and M. Watanabe (2009),  
787 Development of a simple remote sensing evapotranspiration model (Sim-ReSET):  
788 algorithm and model test, *J. Hydrol.*, *376*(3), 476-485, doi:10.1016/j.jhydrol.2009.07.054.
- 789 Tang, R. L., Z. -L. Li, Y. Jia, C. Li, X. Sun, W. P. Kustas, and M. C. Anderson (2011a), An  
790 intercomparison of three remote sensing-based energy balance models using Large  
791 Aperture Scintillometer measurements over a wheat-corn production region, *Remote  
792 Sens. Environ.*, *115*, 3187-3202, doi:10.1016/j.rse.2011.07.004.

- 793 Tang, R. L., Z. -L. Li, and K. S. Chen (2011b), Validating MODIS-derived land surface  
794 evapotranspiration with in situ measurements at two AmeriFlux sites in a semiarid  
795 region, *J. Geophys. Res-Atmo.*, (1984-2012), *116*(D4), doi:10.1029/2010JD014543.
- 796 Tang, R. L., Z. -L. Li, and X. Sun (2013a), Temporal upscaling of instantaneous  
797 evapotranspiration: An intercomparison of four methods using eddy covariance  
798 measurements and MODIS data, *Remote Sens. Environ.*, *138*, 102-118,  
799 doi:10.1016/j.rse.2013.07.001.
- 800 Tang, R. L., Z. -L. Li, and B. Tang (2010), An application of the Ts-VI triangle method with  
801 enhanced edges determination for evapotranspiration estimation from MODIS data in  
802 arid and semi-arid regions: Implementation and validation, *Remote Sens. Environ.*,  
803 *114*(3), 540-551, doi:10.1016/j.rse.2013.07.001.
- 804 Tang, R. L., Z. -L. Li, K. S. Chen, Y. Zhu, and W. Liu (2012), Verification of land surface  
805 evapotranspiration estimation from remote sensing spatial contextual information,  
806 *Hydrol. Process.*, *26*(15), 2283-2293, doi:10.1002/hyp.8341.
- 807 Tang, R. L., Z. -L. Li, Y. Jia, C. Li, K. S. Chen, X. Sun, and J. Lou (2013b), Evaluating one-and  
808 two-source energy balance models in estimating surface evapotranspiration from  
809 Landsat-derived surface temperature and field measurements, *Int. J. Remote Sens.*, *34*(9-  
810 10), 3299-3313, doi:10.1080/01431161.2012.716529.
- 811 Tian, D., and C. J. Martinez (2012), Forecasting reference evapotranspiration using retrospective  
812 forecast analogs in the southeastern United States, *J. Hydrometeorol.*, *13*(6), 1874-1892,  
813 doi:10.1175/JHM-D-12-037.1.
- 814 Todorovic, M. (1999), Single-layer evapotranspiration model with variable canopy resistance, *J.*  
815 *Irrig. Drain. E.*, *125*(5), 235-245, doi:10.1061/(ASCE)0733-9437(1999)125:5(235).
- 816 Trezza, R. (2002), Evapotranspiration using a satellite-based surface energy balance with  
817 standardized ground control, Ph.D. dissertation, USU, Logan, UT, 339 pp.
- 818 Twine, T. E., W. P. Kustas, J. M. Norman, D. R. Cook, P. R. Houser, T. P. Meyers, J. H.  
819 Prueger, P. J. Starks, and M. L. Wesely (2000), Correcting eddy-covariance flux  
820 underestimates over a grassland, *Agr. Forest Meteorol.*, *103*, 279-300, doi:10.1016/S0168-  
821 1923(00)00123-4.
- 822 Van Niel, T. G., T. R. McVicar, M. L. Roderick, A. I. Van Dijk, J. Beringer, L. Hutley, and E.  
823 Van Gorsel (2012), Upscaling latent heat flux for thermal remote sensing studies:  
824 comparison of alternative approaches and correction of bias, *J. Hydrol.*, *468-469*, 35-46,  
825 doi:10.1016/j.jhydrol.2012.08.005.
- 826 Webb, E. K., G. I. Pearman, and R. Leuning (1980), Correction of flux measurements for density  
827 effects due to heat and water vapour transfer, *Q. J. Roy. Meteor. Soc.*, *106*(447), 85-100,  
828 doi:10.1002/qj.49710644707.
- 829 Wilson, K., A. Goldstein, E. Falge, M. Aubinet, D. Baldocchi, P. Berbigier, C. Bernhofer, R.  
830 Ceulemans, H. Dolman, C. Field, A. Grelle, A. Lbrom, B. Law, A. Kowalski, T. Meyers,  
831 J. Moncrieff, R. Monson, W. Oechel, J. Tenhunen, R. Valentini, and S. Verma (2002),  
832 Energy balance closure at FLUXNET sites, *Agr. Forest Meteorol.*, *113*, 223-243,  
833 doi:10.1016/S0168-1923(02)00109-0.

- 834 Xu, T., S. Liu, L. Xu, Y. Chen, Z. Jia, Z. Xu, and J. Nielson (2015), Temporal upscaling and  
835 reconstruction of thermal remotely sensed instantaneous evapotranspiration, *Remote*  
836 *Sens.*, 7, 3400-3425, doi:10.3390/rs70303400.
- 837 Yu, G. R., X. F. Wen, X. M. Sun, B. D. Tanner, X. Lee, and J. Y. Chen (2006), Overview of  
838 ChinaFLUX and evaluation of its eddy covariance measurement, *Agr. Forest Meteor.*,  
839 *137*, 125–137, doi:10.1016/j.agrformet.2006.02.011.
- 840 Yu, Q., G. N. Flerchinger, S. Xu, J. Kozak, L. Ma, and L. Ahuja (2007), Energy balance  
841 simulation of a wheat canopy using the RZ-SHAW (RZWQM-SHAW) model, *Trans.*  
842 *ASABE*, 50(5), 1507-1516, doi: 10.13031/2013.23948.  
843